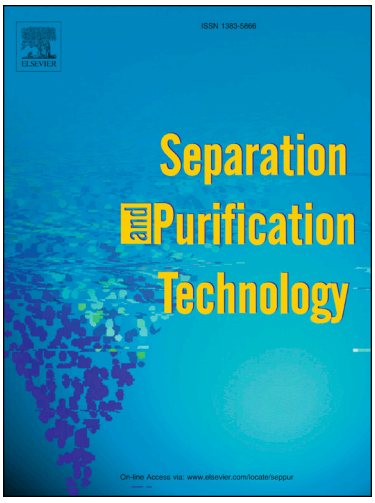

Secondary treated domestic wastewater in reverse electrodialysis: what is the best pre-treatment?

M. Vanoppen, T. van Vooren, L. Gutierrez, M. Roman, L.J-P. Croué, K. Verbeken, J. Philips, A.R.D. Verliefde

PII: S1383-5866(18)33568-8
DOI: https://doi.org/10.1016/j.seppur.2018.12.057
Reference: SEPPUR 15199

To appear in: *Separation and Purification Technology*

Received Date: 10 October 2018
Revised Date: 21 December 2018
Accepted Date: 21 December 2018

Please cite this article as: M. Vanoppen, T. van Vooren, L. Gutierrez, M. Roman, L.J-P. Croué, K. Verbeken, J. Philips, A.R.D. Verliefde, Secondary treated domestic wastewater in reverse electrodialysis: what is the best pre-treatment?, *Separation and Purification Technology* (2018), doi: https://doi.org/10.1016/j.seppur.2018.12.057

Secondary treated domestic wastewater in reverse electrodialysis: what is the best pre-treatment?

M. Vanoppen[1], T. van Vooren[1], L. Gutierrez[1,2], M. Roman[1], L., J-P Croué[3], K. Verbeken[4], J. Philips[5], A.R.D. Verliefde[1]

[1] Particle and Interfacial Technology Group, Faculty of Bioscience Engineering, Ghent University, Ghent, Belgium

[2] Facultad del Mar y Medio Ambiente, Universidad del Pacifico, Ecuador

[3] Institut de Chimie des Milieux et des Materiaux IC2MP UMR 7285 CNRS, Universite de Poitiers, France

[4] Department of Material, Textiles and Chemical Engineering, Ghent University, Technologiepark Ghent, Belgium

[5] Center for Microbial Ecology and Technology, Faculty of Bioscience Engineering, Ghent University, Ghent, Belgium

Abstract art

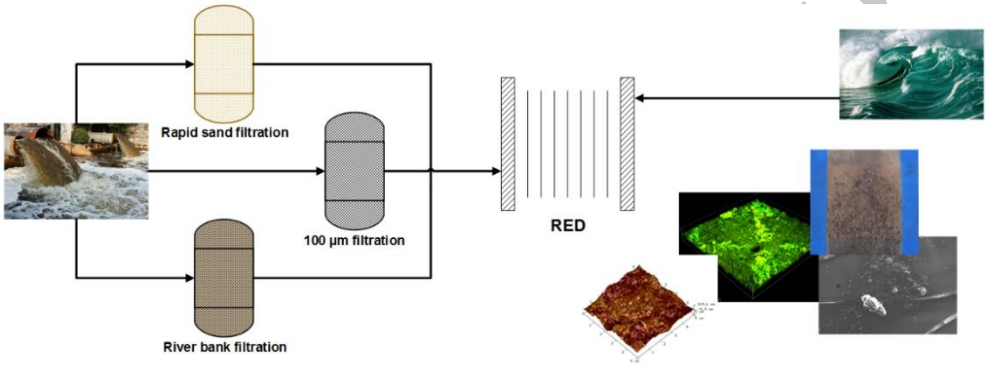

Highlights

- RED-RO is a promising technology for energy-efficient seawater desalination
- Secondary-treated wastewater is a potential low salinity source for RED
- An efficient pre-treatment of wastewater is needed before use in RED
- Rapid sand filtration and 100 µm provide efficient wastewater pre-treatment
- River bank filtration does not provide adequate feed water quality

Abstract

Although Reverse Electrodialysis (RED) is most commonly known as a selective separation technology used for the production of sustainable energy, it can also serve as a valuable pre-desalination tool. By coupling RED to Reverse Osmosis (RO) for seawater desalination: (1) sustainable energy is produced in the RED process and (2) seawater is partially desalinated prior to RO thus, decreasing the energy demand. In this study, secondary-treated wastewater is proposed as the low salinity source in RED and suitable pre-treatment techniques for this effluent are investigated. Although it is generally accepted that RED is less prone to fouling than typical pressure driven membrane processes, results showed that pre-treatment is a key to ensure efficient operation of the wastewater-seawater RED. Both 100 µm filtration and rapid sand filtration proved to be suitable, with an increase in pressure drop of only 0.09-0.18 bar and a permselectivity decrease of only approximately 20% during 40 days of continuous

operation. Conversely, River bank filtration did not perform better than the non-pretreated sample. As such, 100 µm filtration and rapid sand filtration are considered suitable, robust, and cost efficient pre-treatment options for wastewater fed RED, enabling the improvement of the hybrid process of RED-RO seawater desalination.

Keywords

Reverse electrodialysis; wastewater; pre-treatment; desalination

Abbreviations

Abbreviation	Meaning
AFM	Atomic force microscopy
CM	Confocal microscopy
ERS	Electrode rinse solution
QNM	Quantitative nanomechanical mapping
RBF	River bank filter
RED	Reverse electrodialysis
RO	Reverse osmosis
RSF	Rapid sand filter
SEM	Scanning electron microscopy
SW	Seawater
WW	Wastewater
WWTP	Wastewater treatment plant

1. Introduction

Reverse electrodialysis (RED) is an electrochemical membrane technology generally used for the sustainable production of energy from salinity gradients between high salinity (e.g. seawater or brines) and low salinity streams (e.g. river water) [1–3]. This technology consists of alternating anion and cation exchange membranes (AEM and CEM), over which a potential difference is created by the salinity gradient between the feed streams, and has been extensively discussed in literature [4,5]. Recently, a new application of RED, in an RED-reverse osmosis (RO) hybrid, has been suggested [6]. RO is the most widely used technology for drinking water production from seawater. With a typical energy demand of 2-4 kWh/m^3 (at typical seawater salt concentrations of 35 g/L and a recovery of 50%) [7–9] it is an energy intensive process, limiting its applicability in developing regions facing water shortages. Options for decreasing the energy demand of RO are limited, as the thermodynamic limit is 1.06 kWh/m^3 [7,10]. By coupling RED to RO the energy demand can be decreased by: a) producing energy out of the salinity gradient between the RO feed or brine and a low salinity stream and, b) decreasing the seawater salt concentration prior to RO. This RED-RO hybrid system was extensively discussed in Vanoppen et al. (2016) [11].

However, the choice of the low salinity stream for this system is critical, as it does not make sense to use fresh water suitable for drinking water production for this purpose. The use of impaired water (e.g. secondary treated wastewater) is therefore suggested, as this water is generally not used for drinking water production due to legislative, social or cultural barriers. The presence of microcontaminants in impaired also requires additional treatment, increasing energy demand. Combining RED and RO would

provide a double barrier, preventing micropollutants in the impaired water from ending up in the final product water.

Although it is generally accepted that electrochemical membrane systems are less prone to fouling compared to pressure driven membrane systems [4,12,13], an adequate pre-treatment would be required when using impaired water. The most significant fouling in the RED systems used in this study would be of organic and biological nature, because of the use of secondary treated wastewater [13–18]. The risk for scaling is low, since none of the streams are concentrated beyond the initial concentration of the high salinity stream. However, Vermaas et al. (2013) did observe some scaling on the CEM on the seawater side, resulting from the exchange of multivalent ions from river water across that membrane [13]. In a more recent study, Kingsbury et al. (2017) compared the fouling behavior of different natural water pairs in RED. They concluded that natural organic matter (NOM) plays a major role in RED fouling effects, with NOM decreasing the power density up to 43% [15]. Di Salvo et al. (2018) investigated the use of high salinity fishery wastewater and low salinity wastewater after a membrane bioreactor in RED. They observed clear obstruction of the feed channels and adsorption of foulants onto the AEM [19]. Different anti-fouling strategies are reported. Air sparging is an effective way to combat fouling when using real seawater and river water (after pre-treatment by 10 µm filtration) [20] and Moreno et al. (2017) reported the use of CO_2-saturated water as a two-phase flow for successful cleaning and fouling control [21]. Comparable to electrodialysis (ED) reversal, short ED pulses can be used in RED to detach foulants from the membranes [19]. Nevertheless, the literature on fouling in RED remains limited and has mainly focused on stack design [22,23], membrane development [24–26] and cleaning strategies [20,21] to combat fouling. Fouling and water pre-treatment strategies have not received much attention, especially when considering the use of wastewater as the fresh water source in RED.

The selection of a pre-treatment strategy for the impaired water is critical. To allow application of the technology in rural and developing areas, the pre-treatment technology should be simple, robust and cheap. These were the main selection criteria for the technologies tested in this study; none of them requires additional chemicals or extensive process knowledge to operate. Rapid sand filtration (RSF) is a pre-treatment step commonly used in large scale seawater reverse osmosis applications, due to its simplicity, low energy consumption and low operational costs [27]. It can remove suspended solids as small as 0.35 mm by size exclusion and adsorption and can also serve as a substrate to develop a functional microbial biofilm to remove biodegradable compounds and nutrients from the water [27,28]. 100 µm filtration is a conventional membrane filtration, capable of retaining bigger particles (e.g. sand, algae, fibers and debris). The buildup of retained particles on the filter can further increase its efficiency because of secondary filtration. In both RSF and 100 µm filtration, salts, humic acids and microorganisms are not efficiently retained. The costs for both is also similar; ±50 000 EUR for an installation that produces 50 m³/day, with operational costs of 0.1-0.15 EUR/m³ for MF and negligible operational costs for RSF [29,30]. Another option, often used in drinking water production and groundwater recharge and more recently for the removal of micropollutants, is river bank fitration (RBF) [31,32]. In contrast to RSF, flow rates in RBF are significantly lower, while the size distribution of sand particles is considerably wider. Besides simple filtration, the main removal mechanisms are adsorption and biodegradation of solutes by the biologically active medium, thus effectively removing part of the microorganisms and NOM, contrary to the first two techniques [31]. Costs for RBF depend highly on local conditions.

The goal of this study is to identify potential pre-treatment demands for impaired water (i.e. wastewater treatment plant (WWTP) effluent) to be used in RED and to compare different pre-treatment strategies for impaired water and their effect on RED operations. Three different pre-treatment techniques were selected: RSF, 100 µm filtration and RBF, and their performances in terms of maintaining stable RED operation were compared to RED efficiency without pre-treatment. By combining operational parameters (pressure drop, desalination, …) and microscopic analysis (scanning electron microscopy, atomic force microscopy, …), a comprehensive correlation between fouling and pre-treatment type is obtained. This study provides insights into simple, robust and inexpensive treatment methods and their ability to ensure stable long-term RED operation, which is valuable information considering any type of application using ion-exchange membranes with natural water.

2. Materials and methods

2.1. RED set-up

Five cell pairs of alternating AEM and CEM of 10x10 cm² (Fujifilm, The Netherlands) were mounted in a cross-flow stack (REDstack BV, The Netherlands). A schematic overview of the configuration is given in Figure A.1 (Appendix A). Custom made spacers (270 µm, Deukum, Germany) were used to form the flow compartments in between the membranes. Robust CEM were used on both ends of the pile to protect the inner membranes from any possible electrolyte reaction byproducts that could negatively affect them and minimize the transport of ions and organics from the feed solutions to the electrode rinse solution (ERS) and vice versa. Details of the selected membranes can be found in Table A1. In all experiments, the set-ups were identical. To avoid irregularities caused by assembly of the stack, the OCV with synthetic solutions of each separate stack was tested before each experiment (more elaborate information and results in Appendix C).

Platinum coated working electrodes on either side of the stack were connected to a BioLogic VSP potentiostat (Bio-Logic Science Instruments, France) to apply a constant current to the stacks. In cases, a constant current of 50 mA (5 A/m²) was applied to mimic an RED process. Current and potential were recorded every 30 minutes and the open circuit voltage (OCV) was measured every two hours by temporarily switching the current to 0 mA. Ag/AgCl reference electrodes were connected in the end plates (i.e. close to the working electrodes) to measure the stack voltage without any influence of the working electrode losses. A 0.25M NaCl ERS was recirculated along the electrodes.

2.2. Pre-treatment set-up

An **RSF** was constructed using a glass column (H: 0.7m, D: 2.6cm) and pre-filtered sand (Coeck river sand, Brico Plan-it Ghent, Belgium). A grain size of 1-2 mm was used to fill the column to a height of 0.5 m, creating a filter volume of 0.27 L. An average flow rate of 9.5 L/h (17 m/h) was applied to treat each batch of WWTP effluent. After each 60 L batch, the sand filter was backwashed bottom-up using demineralized water until no turbidity was observed in the backwash effluent at the top of the filter.

A commercial filtration unit was used (Purifo 285235, Van Marcke, Belgium) for the **100 µm filtration**. The cylindrical filtration cartridge inside the filter housing had a height of 315 mm and a diameter of 133 mm. Water was fed to the filter, operating inside-out, at an average flow rate of 9.5 L/h. No cleaning of the filter was performed.

To mimic the natural filtration of water through a **river bank**, a polycarbonate tube (H: 1.5 m, D: 19.2 cm) was filled with sand from a natural river bank (Coupure channel, Ghent, Belgium). To allow the biofilm to develop on the filter material, the bed was equilibrated with tap water for 14 days and with the WWTP effluent for an additional 3 days at a flow rate of 0.25 m/d. Batches of the WWTP effluent were then treated at a flow rate of 0.66 L/h (0.55 m/d), flowing from the bottom of the filter to the top to ensure anoxic conditions inside the bank. The pressure drop over the column was monitored using an analog manometer. When the pressure drop exceeded 9 mbar, the bottom (aerobic) layer of the filter was flushed with demineralized water to remove the formed biofilm and accumulated turbidity.

2.3. Feed waters

Seawater from the North Sea and secondary treated WWTP effluent from a domestic wastewater treatment plant (Aquafin, Ghent, Belgium) were selected as feed waters. The seawater was pre-treated by sand filtration, bead filtration (Polygeyser Bead Filter, Aquaculture Systems Technologies, USA) and UV and stored in a 29 m³ storage tank (Department of Animal Sciences and Aquatic Ecology, Ghent University). As no other disinfection was applied, some biological growth and activity is expected in the seawater once it is fed to the RED stacks. The average properties of the feed waters can be found in Table 1. The high variation, especially for the wastewater, can be explained by varying weather conditions and timing of the sample taking.

Table 1. Average properties of the feed waters in both runs (standard deviations, n = 12)

		σ			T			Na			K			Ca			Mg			TOC		
		(mS/cm)			(°C)			mg/L			mg/L			mg/L			mg/L			mg/L		
SW	**Run 1**	48.35	±	5.1	19	±	1	11633*	±	3849	468	±	96	586	±	81	890	±	308	1.8	±	0.0
	Run 2	58.38	±	2.95	20	±	1	8319*	±	484	268	±	49	392	±	71	1165	±	197			
WWTP effluent	**Run 1**	1.13	±	0.39	19	±	1	113	±	32	21	±	9	96	±	27	10	±	3	3.9	±	2.7
	Run 2	1.13	±	0.28	21	±	1	212	±	327	22	±	7	104	±	30	11	±	2	3.7	±	1.3

* Estimates, sample concentrations were above the highest standard. These values are used as an indication to avoid over dilution of the sample.

2.4. Experimental protocol

Two testing periods (runs) with two and three parallel tests were performed to compare the different pre-treatment methods. In the first six weeks-testing period (November-December 2016), RSF and 100 µm filtration were tested in parallel and compared to a reference stack receiving unpre-treated WWTP effluent. In the second six weeks-testing period (March-April 2017), RBF was compared to a second reference. Each week, two batches of 60 L were fed to the RED stacks. The pre-treatment was performed in batch mode, separated from the RED set-up (see Figure 1). In total, 720 L of both WWTP effluent and seawater were pre-treated and fed to each RED stack. Fresh feed water was collected twice per week and distributed amongst the parallel testing trains, to eliminate any influence of batch composition when comparing the different pre-treatments. All experiments were performed at room temperature. The whole system was never shut down for more than an hour during batch switches.

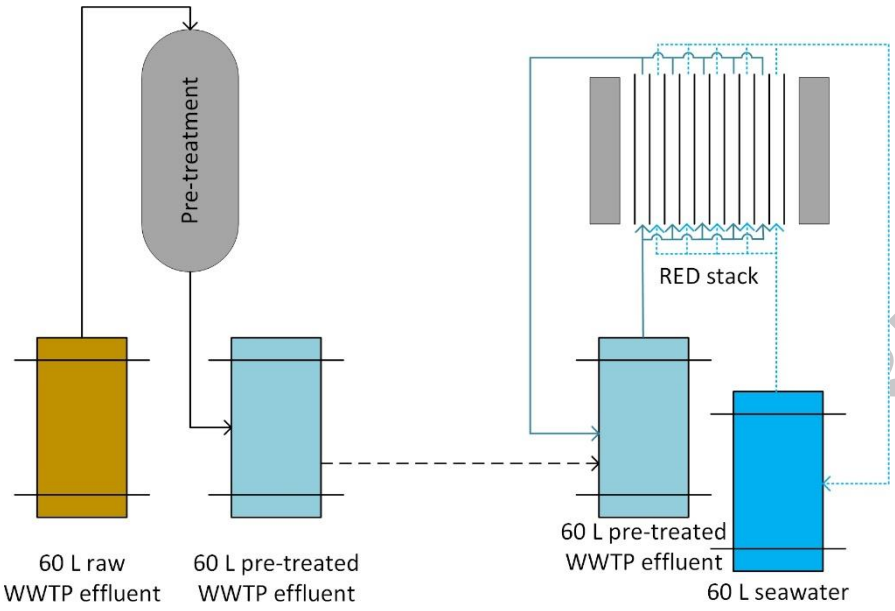

Figure 1. Schematic overview of the experimental set-up in which WWTP effluent is treated in batch before being fed to the batch RED process (WWTP = wastewater treatment plant, RED = reverse electrodialysis)

2.4.1.Cleaning protocols

Whenever the pressure drop over a compartment exceeded 1 bar, a cleaning was initiated. As the main fouling type expected is organic fouling, a first cleaning protocol tested was a flush with NaOH (2L, 0.1M, recirculated for 30 minutes), preceded and followed by a flush with 1L of demineralized water. Although this resulted in an initial decrease of the pressure drop, it increased again rapidly in the wastewater compartment of the reference stack. For the second cleaning, an acid cleaning was included as well (0.1M HCl). In both of these first cleaning protocols, the normal flow rate (0.7 cm/s) was maintained, as well as the normal flow direction. During the second set of experiments, to ensure optimal cleaning of the compartments, NaOH and HCl flushes were done at doubled flow rate (1.5 cm/s) and in the opposite flow direction (outlet to inlet). This protocol was applied to the rest of the cleanings.

2.5. Water quality analysis and chemical analysis of the biofilm

Samples of both waters were taken at the beginning and end of each batch. Conductivity and temperature were measured using a conventional conductivity probe (C3020 controller with SK10T probe, Consort, BE). The concentrations of the major cations (Na^+, K^+, Ca^{2+} and Mg^{2+}) was determined using ICP-OES (Inductively Coupled Plasma – Optical Emission Spectroscopy, Varian VISTA-MPX, USA). The pressure drop over the different compartments was measured daily, using a pressure difference meter (JUMO MIDAS DP10 401050, JUMO GmbH & Co., DE).

For chemical analysis of the deposits on the membrane, pieces of 1.5x1.5 cm^2 were scraped using a scalpel under aseptic conditions. The scrapings were immediately transferred to 50 mL PBS buffer. A comprehensive overview of all sampling spots on the membranes can be found in Appendix B (Figure B.1). Chemical analysis was performed at the inlet, middle and outlet of each membrane on both the wastewater and seawater compartment side. Samples of the respective spacers (1.5x1.5 cm^2) were also immersed into the same PBS buffer solution and sonicated (twice for 30 seconds) to include any deposit

attached to the spacer material. ATP (adenosine triphosphate) and carbohydrate analysis were performed on these samples to assess the biological presence and activity of the biofilm. ATP was analyzed using a BacTiter-Glo™ kit (Promega Corporation, USA) and carbohydrates were determined according to the Dubois method [33].

2.6. Microscopy analysis of fouled membranes

After the experiments, the fouling of the membranes was analyzed microscopically. A membrane sample was cut from the middle of the membrane. The middle cell pair was selected. Biofilms were examined using confocal microscopy (CM), scanning electron microscopy (SEM) and quantitative nanomechanical mapping (QNM).

2.6.1. Confocal microscopy

Membrane pieces were fixed with glutaraldehyde and stained using SYTO9 (green) and propidium iodide (red) (Live/Dead BacLight Bacterial Viability Kits, Life Technologies), as described before [34]. Biofilms were visualized using a Nikon A1R confocal laser scanning microscope (Nikon Instruments Europe B.V., NL), as previously described [35]. Unstained and stained virgin membrane samples were used as controls. Unstained membranes did not light up, showing that the membranes were not autofluorescent. For the stained virgin CEM membrane, a strong signal mainly from the red laser was obtained, while the stained AEM membrane barely showed a signal (Figure in Appendix G). For this reason, images of CEM were only recorded with the green laser (viable cells). All images were recorded with the same laser setting to allow comparison of the light intensity between the different images.

2.6.2.Scanning electron microscopy

The surface of the membranes was visualized using scanning electron miscroscopy (FEG SEM JSM-7600F, JEOL, USA), after fixation of the membranes by the protocol described by Arends et al. (2012) [36].

2.6.3.Quantitative nanomechanical mapping

A Dimension FastScan Atomic Force Microscope (Bruker, USA) with an FastScan Head were used for QNM analysis in electrolyte solution. Electrolyte solutions (1 mM NaCl) for QNM experiments were prepared with MilliQ water (18 MΩ.cm resistivity) and analytical grade reagents, and then filtered through a 0.22 µm membrane. Sharp Silicon Nitride Cantilever AFM probes (SNL-10 A, Bruker, USA) were selected based on the soft polymeric characteristics of the membrane samples and foulant layers, as described in Gutierrez et al. (2018) [37]. Briefly, the spring constant of these cantilevers (i.e., k: 0.35 N/m) would allow enough membrane sample deformation without structurally compromising the sample, while still retaining the sensitivity of the cantilever. The deflection sensitivity of the AFM probes was calculated in air conditions and using mica as a control surface; the spring constant (k) was measured using the Thermal Tuning method in accordance to Hooke's law [38]. The radius of curvature of the probes was calculated by scanning a titanium model surface (Bruker, USA) in air conditions using the Tip Qualification function (NanoScope Analysis Software V1.5, Bruker, USA). Membrane samples were placed on a glass slide using double-sided tape and inspected using the AFM high resolution camera (Appendix J). Areas ranging from 1×1 µm to 10×10 µm (e.g., membrane surface or foulant layers) were randomly selected for QNM analysis, and acquired at a scan rate of 0.5 kHz and at 512 samples/line. The ScanAssyst Auto Control was set ON; thus, allowing Peak Force Setpoint to be automatically controlled by the software. The following parameters (channels) were recorded during

QNM analysis: topography, adhesion, deformation, dissipation, DMT Modulus, and LogDMT Modulus [37]. Briefly, the deformation channel records the deformation (nm) of the polymeric structures of the membrane or foulant layer caused by the AFM probe during approaching regime [39]. The adhesion channel measures the adhesion force (nN) between the sample and AFM probe during retracting regime (i.e., indicating the strength of the bond) [40]. During this process, the Young's modulus describing tensile elasticity (i.e., material stiffness) is calculated using Derjaguin-Muller-Toporov (DMT) model, and finally expressed as DMT Modulus [41]. LogDMT Modulus is calculated as the logarithm of the elastic modulus of the sample based on the DMT model. The dissipation channel describes the mechanical energy lost per approaching-retracting cycle; specifically, the hysteresis between approaching and retracting curve (e.g., pure elastic deformation of the membrane corresponds to very low dissipation, while plastic deformation corresponds to higher dissipation) [42]. Every nanomechanical property was statistically processed by Image Quadratic Mean (Rq) analysis, where mean (μ) and variance (σ) were calculated. Also, topographic and phase analysis of foulant layers and membrane samples were performed by Soft-Tapping ModeTM (Bruker, USA) using TESPA AFM probes (silicon tip, k: 42 N/m, f: 320 kHz, Bruker, USA) to provide supplementary information on the characteristics of samples. The coverage of the membrane surface by the fouling layer was determined by analyzing the images using ImageJ software (National Institute of Health-USA). A threshold filter was used to discriminate the membrane surface from fouling layers.

2.6. Membrane permselectivity and power density

2.6.1.Permselectivity

The permselectivity (α) describes the ability of the ion exchange membrane to distinguish between co-ions and counter-ions, thus providing a good indication of the integrity of the membrane. Fouling or membrane damage can drastically influence this parameter. The apparent permselectivity is calculated by comparing OCV measurements to the theoretical OCV as predicted by the Nernst equation. When the membrane becomes more permeable to co-ions, the potential built up across the membrane and thus the OCV decreases relative to the expected value, as expressed in equations 1 and 2.

$$\alpha = \frac{E_{OCV,m}}{E_{OCV,th}} \tag{1}$$

$$E_{OCV,th} = N_m \cdot \frac{R \cdot T}{n \cdot F} \cdot ln\left(\frac{\gamma_{sea} \cdot c_{sea}}{\gamma_{waste} \cdot c_{waste}}\right) \tag{2}$$

With $E_{OCV,m}$ (V) the measured OCV and $E_{OCV,th}$ (V) the theoretical OCV, based on the amount of membranes N_m (-). R (8.314 J/(mol·K) is the universal gas constant, T (K) is the absolute temperature, F (96485 C/mol) is the Faraday constant, n (-) is the valence of the ionic species and c (mol/L) is the concentration of both feed waters. The presence of multivalent ions, which can decrease the power production through ion-exchange across the membranes, was taken into account in the same way as discussed in Kingsbury et al. (2017) [15]. Activity coefficients were calculated using the Debye-Hückel theory as adapted by Davies [43]. This results in a theoretical OCV of 1 120 mV for the first set of experiments and 1 568 mV for the second set. The latter value is slightly higher because of the higher conductivity of the seawater during this period.

2.6.2.Power density

The gross power density (i.e. the power produced by the stack) was calculated based on the measured current and potential difference (equation 3). However, part of the power would be needed for pumping of the feed streams, resulting in the net power density (equation 4).

$$Pd_{gross} = \frac{I \cdot U}{N_m \cdot A} \quad (3)$$

$$Pd_{net} = P_{gross} - \frac{\Delta p_{sea} \cdot Q_{sea} + \Delta p_{waste} \cdot Q_{waste}}{N_m \cdot A} \quad (4)$$

In which Pd (W/m²) is the power density, I (A), U (V) is the potential difference, Δp (Pa) is the pressure drop over the compartments, Q (m³/s) is the flow rate and A (m²) is the active surface area of one membrane.

3. Results and discussion

3.1. Pressure drop and power density

The development of the pressure drop over the different compartments is shown in Figure 2. In the first run (RSF, 100 µm filter and reference), the pressure drop over the wastewater compartment of the reference stack (receiving raw wastewater effluent) increased rapidly. After 11 days of operation, it exceeded 1 bar for the first time, triggering the first cleaning action. After an initial, limited decrease in the pressure drop, it increased again, requiring another cleaning after 31 days of operation. This indicates the rapid formation of an irreversible fouling layer on the membrane. The pressure drop over the wastewater compartment fed with pre-treated water increased slightly over the course of 6 weeks; from 0.03 to 0.12 bar for the 100 µm filter and from 0.04 to 0.22 bar for the RSF.

The pressure drop over the seawater compartment during these 6 weeks was very similar for all three stacks, up until approximately day 32. After that day, the pressure drop in the reference stacks continued to increase, but the pressure drop in both other stacks gradually decreased. A possible explanation for this observation would be a slow detachment of the biofilm over time (i.e. reversible adsorption). Potentially, the pre-treated nature of the water resulted in the formation of a loose, unstable biofilm that started detaching after a certain pressure drop was reached. However, this hypothesis can at this moment not be validated by the gathered data and more experimental evidence is needed to corroborate it. The pre-treatment protocols were executed as before, the integrity of all stacks was double-checked, and none of the other parameters monitored showed any deviations. In both stacks, the pressure drop reached a maximum of 0.7 bar around day 32 before dropping back to 0.09 bar by the end of the experiment.

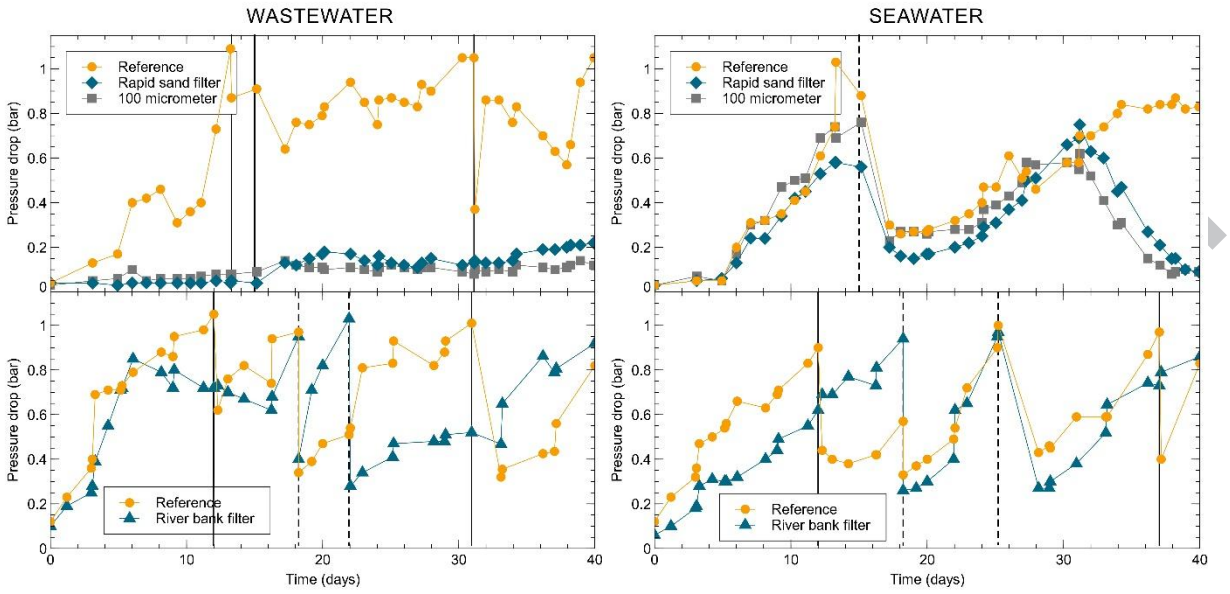

Figure 2. Pressure drop over the wastewater compartment in RED following the different pre-treatment options for the wastewater and seawater compartments, with the first run on the top and the second run on the bottom of the figure. Cleanings were performed when pressure drops in a given compartment approached/exceeded 1 bar. Solid lines represent cleanings of the reference stack while dashed lines represent cleanings of the treatments with or without the reference (depending if the reference stack's pressure drop approached/exceeded 1 bar at that moment).

In the first half of this run (i.e. where the RBF surely worked properly), the pressure drop over both stacks increased in a similar way. After the complete cleaning of both stacks around day 22 however, the pressure drop over the wastewater compartment in the stack fed after RBF seemed to increase more slowly, although it was still significantly higher than the pressure drop recorded after pre-treatment with RSF or 100µm filtration. In the seawater compartment, the pressure drop profile was comparable to the first run.

These results reflect in the gross and net power density. The gross power density was comparable for all treatments and decreased slightly during the experiments, with an average of 0.25±0.03 W/m² in the first run and 0.21±0.04 W/m² in the second run. This variation would be due to a changing OCV, caused by membrane fouling, and changes in the feed water composition. Both affect the amount of energy that could be produced. However, the pressure drop had a significant influence on the net energy that could be produced by increasing the pumping energy needed. This pumping energy increased 22-fold over the course of the experiment for the reference stack in the first run, while it only increased 5 and 4-fold after RSF and 100 µm filtration respectively. The increase in the second run is 4 and 10-fold for the reference and RBF pre-treated stack, respectively. These lower values, especially for the second reference, can be attributed to the more frequent cleaning and higher initial pressure drop during these experiments.

The maximum power densities recorded in this study (given in Appendix D) are low compared to those reported in literature [25,44,45] but in line with a complementary study performed by Kingsbury et al. (2018) [15]. Although it was reported that a minimum net power density of 2.2 W/m² is needed to make RED commercially attractive as a source of renewable energy [46], the focus in this investigation was on comparing pre-treatment techniques and developing a system for seawater desalination. Many options

to improve power density are currently being investigated, including membrane profiling [24,25,44], conductive spacers [22] and alternative modes of operation [23,45].

3.2. *Permselectivity*

The average apparent permselectivity for each batch, calculated based on equations 1 and 2, is shown in Fig. 4. As (often large) charged organic molecules are attracted to and subsequently adsorbed onto the membranes, they can occupy and shield part of the membrane charge, decreasing the number of functional groups available for transport and the charge density responsible for repelling co-ions from the membrane surface [27]. This explains why the permselectivity was lower for the reference case compared to the pre-treated cases in the first run. There was no distinguishable difference between RSF and 100 µm filtration, indicating a very similar fouling behavior, which confirmed the pressure drop observations. However, at the end of run 1, all stacks reached the same permselectivity, indicating that the effect of fouling on this parameter is rather small and all stacks reached a similar equilibrium. Although the initial drop in permselectivity was less clear, these results are similar to those of Vermaas et al. (2013), who compared the use of profiled membrane and spacers in RED on river water and seawater [1].

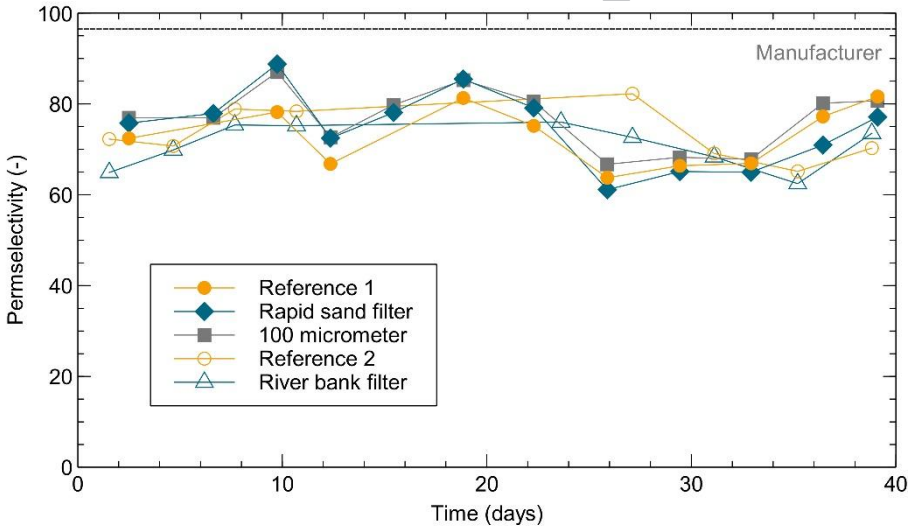

Figure 3. Permselectivity in all five experiments compared to the permselectivity under ideal circumstances given by the manufacturer. The permselectivity calculation takes into account the measured concentrations at the start of each batch and the losses due to uphill transport of multivalent ions.

Overall, no clear decrease in permselectivity was measured and the observed variation is explained largely by the variation in feed water composition. No clear effect of the cleanings is observed either, indicating that operation is influenced mostly by the mechanical clogging of the system, resulting in increased pressure drops, rather than by a decrease in membrane functionality.

3.3. Membrane autopsy

3.3.1.Chemical analysis

After 6 weeks, the stacks were opened and the membranes were removed for inspection. Visually, the color of all AEM had changed from the original yellow/beige color to a darker, browner color, indicating the adsorption of NOM onto the membranes (Figure E.1). The CEM on the other hand had retained their original whitish color, indicating low organic adsorption. The difference between organic adsorption level in CEM and AEM is generally explained by the positive charge of the AEM. As NOM mainly consists of negatively charged compounds, electrostatic attraction dictates their preferable adsorption onto the AEM.

ATP was determined to assess the amount of metabolically active cells present on the membranes and thus the activity of the fouling biofilm. Similarly, carbohydrates were analyzed to indicate the presence of a biofilm on different sites on the membranes. In all runs, ATP concentrations were highest in the seawater compartment, which could indicate biological growth in the seawater during storage (Figure 4) and increased growth during the experiment because of a lack of pre-treatment of the seawater prior to the RED experiments. ATP concentrations during the second run were considerably lower, which indicates that although fouling was more severe, there were less viable organisms present. Carbohydrate concentrations were comparable, but more evenly distributed over the membranes. This indicates that in the second run, a structurally different kind of biofilm was formed, possible due to the change in seasons and the subsequent effect on microbial communities in the effluent.

Overall, ATP and carbohydrate concentrations were highest at the inlet and (to a lesser extent) the outlet. Due to the changing hydraulic conditions at inlets and outlets, particles would easily get trapped in the spacers and a biofilm would easily form. This was also confirmed visually (Figure F.1 and F.2). This can be attributed to the stack design. In order to close the stack and prevent leaks, membranes and spacers are pressed together by a metal frame, bolted in the four corners of the membranes. The spacers form the different flow compartments as they are blocked of on two sides by a different material, making the spacers slightly thicker on these sides (see pictures in appendix E and F). This causes the pressure on the inlet and outlet to be slightly greater when bolted together than in the rest of the membrane and can cause (organic) particles to get stuck here. This is confirmed by the observation that the band of fouling formed at the inlet is approximately the same width as the blue reinforced parts of the spacers. As a result, more organic material is trapped and a biofilm is developed more easily where the pressure is higher. In the center of the membrane however, this stress is lower, creating an unobstructed flow-path for the feed water.

As expected, in the first run ATP was higher in the reference stack compared to the stacks receiving pre-treated water, where similar values were measured. In the second run, there was no discernable difference between the reference and the pre-treated stack, which can (partially) explain the similar overall behavior of both stacks. For carbohydrates, it was not possible to identify clear trends. This indicates that the amount of active biomass was significantly higher in seawater (ATP data), while the amount of inactive biomass remained similar in both streams (carbohydrate data).

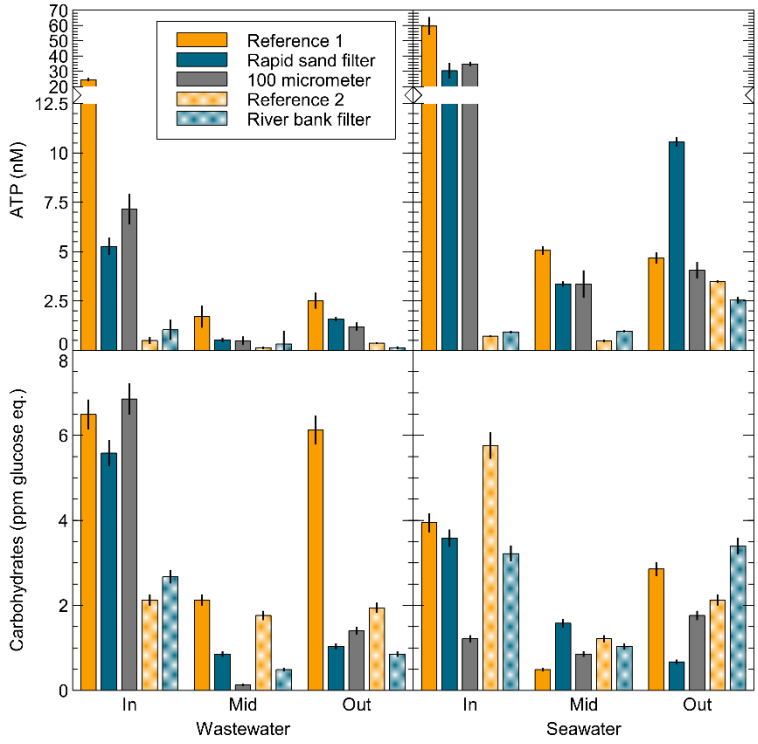

Figure 4. Adenosine triphosphate (ATP, top) and carbohydrate (bottom) analysis of the membrane surfaces for all experiments on the wastewater (left) and seawater (right) side. Error bars represent standard deviations on analytical replicates (n=3).

3.3.2.Microscopy analysis

The center of both membrane types at both seawater and wastewater side was subjected to SEM, CM and QNM. All analyses were also conducted on virgin (i.e. unused) membranes (Figure G.1). In SEM, very little contamination was found on the virgin membranes. The structures observed were the coated fibers within the membrane structure. Some green fluorescence from the virgin AEM and some green and red fluorescence from the CEM were recorded by CM. This was taken into account when interpreting the CM results.

Figure 5 and Figure 6 show the CM and SEM results for the wastewater side of both AEM and CEM. Since seawater was not pre-treated and no differences between the different treatments were observed, these results are included in Appendix H (Figure H.1 and H.2). All SEM pictures are shown at the same scale, providing an overview of a piece of membrane of 455x342 µm². Surprisingly, more patches of fouling were observed on the CEM membranes. However, confocal microscopy shows that these patches do not consist of a living biofilm. Potentially, particles stuck in the spacers or dead parts of the biofilm from the AEM were present on the CEM due to the opening of the stack and the separation of the CEM, AEM and spacer. This is also consistent with the QNM results, discussed later. The CM images all have a magnification of only 10X, providing a wide overview of a patch of 1 273x1 273 µm² of membrane. Confocal images of AEM were recorded with both green and red lasers, but images mainly colored green, suggesting that the biofilms were dominated by viable cells (thickest biofilm for RBF). CEM were only visualized with the green laser (since the red stain also adsorbed to the membrane itself, as was concluded from stained virgin membranes). Green patches were seen on CEM membranes,

indicating the presence of viable cells as well (the most considerable biofouling was observed on reference 2), but were less pronounced than on the AEM.

Both on the SEM and CM pictures of the RBF pre-treatment, a severe fouling layer was observed. As all confocal images were produced under the same lighting settings, the brightness of the green color can be used as an indication of the density of the living biofilm, which was clearly higher in this case. However, this contradicts the ATP analysis, which indicated a lower amount of biological activity for the RBF treatment. This could indicate that the biofilm formed after RBF was structurally different.

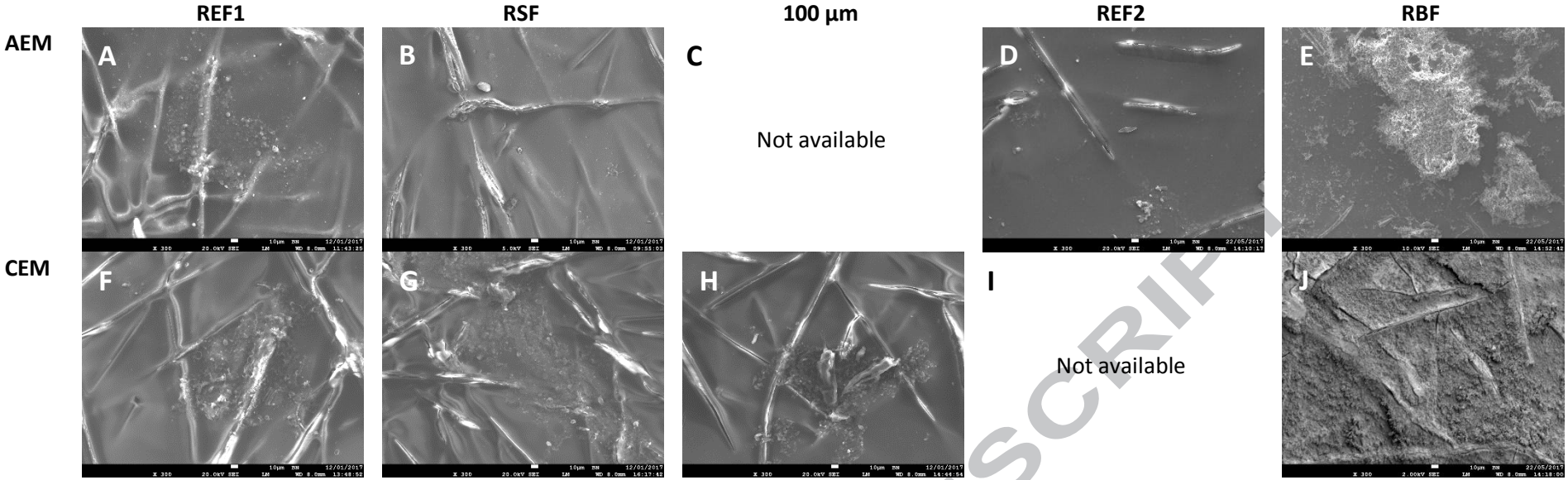

Figure 5. Scanning electron microscopy images of the wastewater side of all membranes (REF1 = reference 1, RSF = rapid sand filter, 100µm = 100 µm filter, REF2 = reference 2, RBF = river bank filter). Two images are unavailable due to technical issues with the pre-treatment for the analysis.

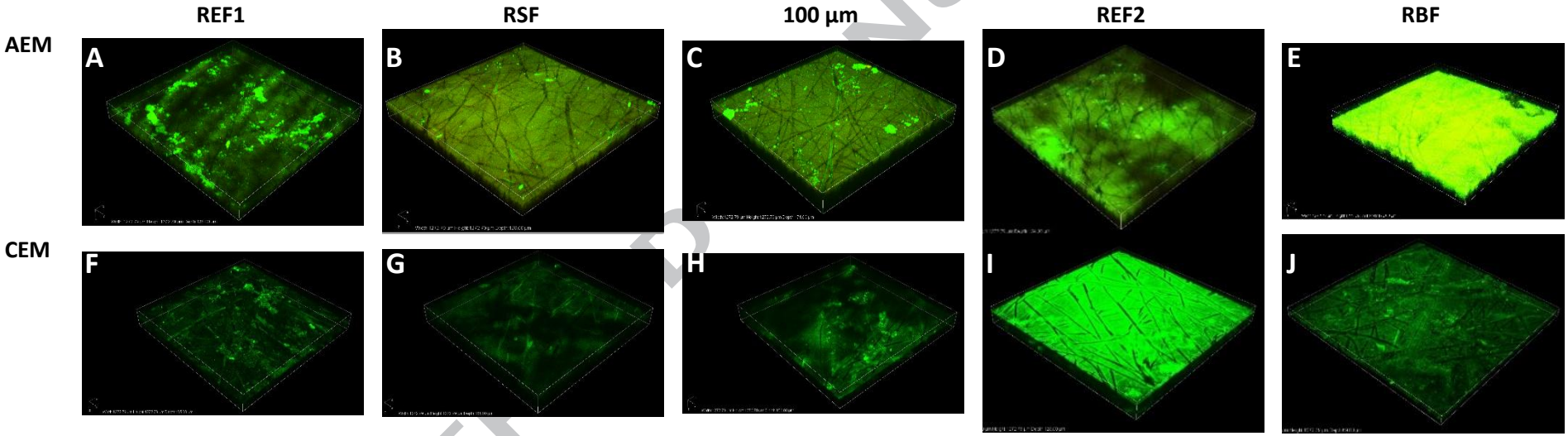

Figure 6. Confocal microscopy images of the wastewater side of all membranes (REF1 = reference 1, RSF = rapid sand filter, 100 µm = 100 µm filter, REF2 = reference 2, RBF = river bank filter).

Although CM and SEM provide a good overview of the overall fouling behavior of the different membranes in different conditions, these results are qualitative in nature. A quantification was achieved through the QNM analysis. An overview of the results is shown in Table 2, and the analysis of the virgin membranes is discussed in more detail in Appendix I.

The severe fouling observed on the reference membranes (Figure 5 and Figure 6, A, F, D and I) was confirmed by QNM, with 14-37% of the membrane covered by fouling (Figure H.1). Due to the high heterogeneity in the surface distribution of these fouling layers, no significant statistical difference was observed between CEM and AEM, neither in seawater or wastewater samples. This confirms the SEM and CM analysis, where no clear difference between the membranes is observed either. Topographic images of the fouling layers by tapping mode showed high R_{RMS} of up to 415 nm while phase images (i.e. chemical mapping of surfaces based on material differences) indicated surfaces with highly heterogeneous characteristics.

Table 2. Roughness, DMT modulus, adhesion, deformation, dissipation and fouling coverage for the different membranes and different operating conditions as determined by QNM.

		R_{RMS} (nm) (n=10)	n	Mean log DMT modulus (Log[Pa]±)	Adhesion (nN)	Deformation (nm)	Dissipation (eV±)	Foulant coverage (%)
Virgin	**AEM**	4.7 ± 0.9	10	0.105	1.05	5.41	273	0
	CEM	7.9 ± 1.3	10	0.151	0.21	6.72	459	0
Reference membrane	**AEM**	No clean membrane surface recorded at the nanoscale						
	CEM	16 – 45.7	4	0.257	3.04	7.12	988	0
Reference* fouling	**AEM**	85 – 415	40	0.101 – 0.309	3.05 – 10.4	2.5 – 22.4	787 – 5091	14 – 37
	CEM							
100 µm	**AEM**	43 – 361	14	0.124 – 0.462	2.41 – 7.94	5.7 – 14.2	581 – 3791	19 – 32
	CEM		12					
RSF	**AEM**	18 – 162	10	0.109 – 0.248	3.05 – 8.45	7.7 – 12.6	832 – 2945	3 – 12
	CEM		13					
RBF	**AEM**	25 - 201	10	0.138 – 0.315	4.15 – 9.75	4.9 – 21.3	641 - 3652	5 – 15
	CEM		14					

* No statistical difference between AEM and CEM

QNM analysis was also performed on the fouling layers of the reference membranes (Figure I.1). The morphology and nanomechanical properties of foulant layers highly differed from those of virgin membranes and could not be statistically analyzed by probability density functions due to their high heterogeneity. The calculated parameters (Table 2) indicate stiff, low elastic properties, and highly adhesive fouling layers. The presence of these foulants after extended operation and chemical cleaning and their high adhesion would be a nanoscale evidence of irreversible fouling (adsorption) [48,49]. Additionally, previous investigations have also observed foulants of lower elastic modulus compared to virgin membranes [50]. When analyzing apparently clean areas on the reference membranes (i.e. areas showing no adsorbed fouling layers at the microscale were exclusively scanned), the AEM still exhibited fouling with a R_{RMS} of 16.8-45.7 nm, indicating that fouling covers the membrane surface at a nanoscale (Figure 7 left). Approximately 20% of the CEM samples (both wastewater and seawater side) displayed the characteristic polymeric structure seen in the virgin membranes, indicating around 80% of the

membrane surface covered by fouling (Figure 7 middle). However, the mean adhesion and dissipation of these CEM surfaces were 3.04 nN and 988 eV±; thus, differing from CEM-virgin and indicating changes in surface properties (i.e., lower elasticity and higher adhesion) possibly due to foulant adsorption and chemical cleaning. Previous investigations have recorded similar changes in membrane surface characteristics caused by fouling and extended operation [37].

Membranes subjected to feed pre-treated by RBF showed no significant difference in any of the QNM parameters compared to the reference membranes. This, together with the clear more severe fouling observed in the SEM and CM analysis (Figure 5 and Figure 6, E and J), confirms that RBF pre-treatment is insufficient. However, membranes subjected to feeds pre-treated by 100 µm filtration and RSF showed a significantly lower presence of fouling layers at the microscale (i.e., recorded by the AFM high-resolution camera). Approximately 3-15% of the surface area of the membranes was covered by fouling layers, and their nanomechanical properties were highly heterogeneous and similar to those found on the reference membranes. Specifically, foulants of high DMT modulus, adhesion, and dissipation (i.e., stiff, low elasticity, and highly adhesive) were recorded. Apparently clean membrane surfaces were also scanned in 2×2 and 5×5 µm areas. No clean membrane surface was detected in any of the AEM samples. However, approximately 67% of CEM images showed clean membrane surfaces (Figure 7 right). This trend, also observed in the reference membranes, would be explained by the stronger interactions between positively-charged functional groups on AEMs and negatively-charged organics; thus, leading to conditioning film formation [51].

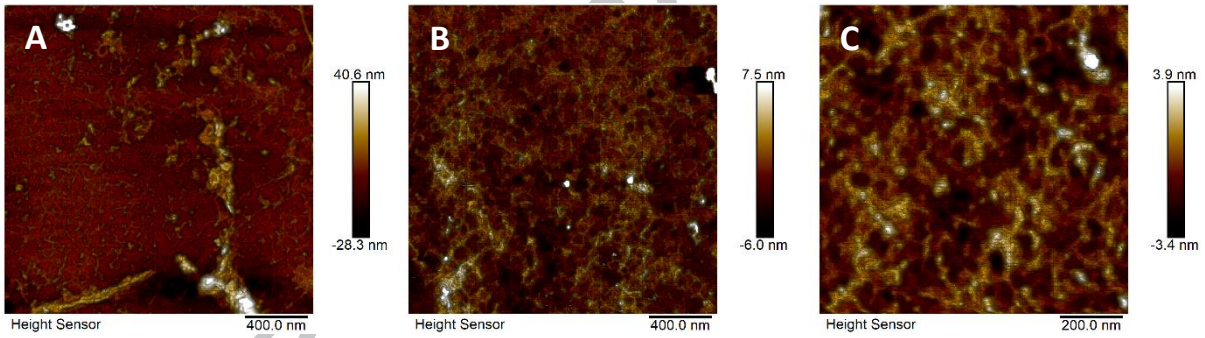

Figure 7. Height sensor of an apparently clean membrane surface on (A) Reference AEM-SW, (B) Reference CEM-SW, and (C) 100 µm Filter CEM-WW. The analysis at the nanoscale revealed that only CEMs showed polymeric structures corresponding to membrane surface.

On all membranes, the presence of bacteria and a biofilm was confirmed. However, the presence was significantly lower after 100 µm filtration and SRF compared to the reference samples. On seawater membrane samples, rod-shaped bacteria of 1.42±0.15 µm and possible amoeba of 7.82±0.87 µm were observed (n=10) (Figure 8 left). On wastewater samples, only bacteria of 2.02±0.12 µm were recorded (n=10) (Figure 8 right). The mean adhesion, dissipation, and modulus of bacteria were even higher than those of the surrounding biofilm. These results indicate a stiff, adhesive, and rather plastic bacterial membrane.

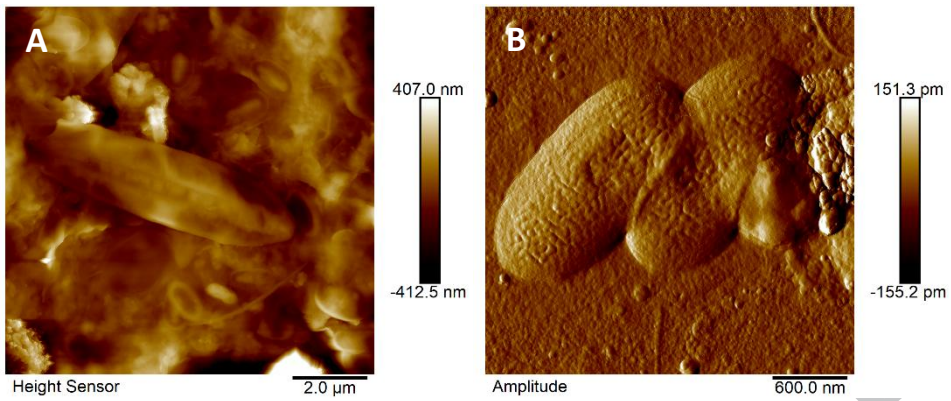

Figure 8. (A) high sensor image of RSF CEM (seawater side) and (B) amplitude image of 100 µm filtration CEM (wastewater side).

3.4. RBF as pre-treatment

River bank filtration has shown its merits in the treatment of natural waters. It is used as a pre-treatment in drinking water production [32] and investigated for its ability to remove micropollutants from e.g. river water [52,53]. However, to the best of our knowledge, is has never been used as a direct treatment method for WWTP effluent. Van Houtte & Verbauwhede (2008) discussed long term infiltration of WWTP effluent in sand dunes for indirect potable reuse, but only after UF and RO treatment of the effluent [17].

Our results indicate that the application of RBF for WWTP effluent treatment is not straightforward. Similar column experiments with river bank sediment have been performed successfully before, but never on WWTP effluent [52,53]. The column used in this study had been used with success before for the treatment of river water. During that time, a microbial community had successfully developed on the filter media, a process that can take up to 3-4 months [54]. Potentially, the community adapted to the river water started to deteriorate once operations were switched to the WWTP effluent causing the RBF to fail over time as the microbial community was unable to adapt to the new conditions. Although the system did seem to work well in the first few weeks, for RBF to be a truly successful, robust pre-treatment option for WWTP effluent, more research is needed into the necessary characteristics of the sediment, biology and operational parameters.

4. Conclusions

RED has the potential to decrease seawater RO desalination energy demand, by the production of energy from the selective separation of feeds with different salinities. One proposed low salinity feed stream is WWTP effluent. Different pre-treatments for wastewater used in RED were compared to non-pre-treated conditions, when real seawater and wastewater are used. This study has clearly proven that adequate pre-treatment is necessary to ensure efficient operation of the RED system.

Both 100 µm filtration and rapid sand filtration were able to significantly reduce fouling on the membrane surfaces, resulting in lower pressure drops, lower frequency of cleanings, and a higher permselectivity. Results point towards a less prolific biofilm formation and less pronounced clogging of the feed channels. River bank filtration showed no improvement compared to no pre-treatment at all, which might be related to the difficulties in reproducing this technology on a lab scale and the nature of the feed water (i.e. wastewater). In general, the inlets and outlets of the spacer filled channels showed

to be the critical weak spot in all treatments, providing ideal circumstances for the development of a biofilm.

5. Acknowledgements

This project has received funding from the European Union's Horizon 2020 research and innovation programme under grant agreement No 685579.

Declarations of interest: none.

6. References

[1] A. Daniilidis, R. Herber, D. a. Vermaas, Upscale potential and financial feasibility of a reverse electrodialysis power plant, Appl. Energy. 119 (2014) 257–265. doi:10.1016/j.apenergy.2013.12.066.

[2] A. Cipollina, G. Micale, A. Tamburini, M. Tedesco, L. Gurreri, J. Veerman, S. Grasman, Reverse electrodialysis: applications, in: A. Cipollina, G. Micale (Eds.), Sustain. Energy from Salin. Gradients, 1st ed., Woodhead Publishing-Elsevier, London, 2016: pp. 135–180.

[3] J. Veerman, M. Saakes, S.J. Metz, G.J. Harmsen, Electrical power from sea and river water by reverse electrodialysis: A first step from the laboratory to a real power plant, Environ. Sci. Technol. 44 (2010) 9207–9212. doi:10.1021/es1009345.

[4] J.W. Post, J. Veerman, H.V.M. Hamelers, G.J.W. Euverink, S.J. Metz, K. Nymeijer, C.J.N. Buisman, Salinity-gradient power: Evaluation of pressure-retarded osmosis and reverse electrodialysis, J. Memb. Sci. 288 (2007) 218–230. doi:10.1016/j.memsci.2006.11.018.

[5] D.A. Vermaas, E. Guler, M. Saakes, K. Nijmeijer, Theoretical power density from salinity gradients using reverse electrodialysis, Energy Procedia. 20 (2012) 170–184. doi:10.1016/j.egypro.2012.03.018.

[6] W. Li, W.B. Krantz, E.R. Cornelissen, J.W. Post, A.R.D. Verliefde, C.Y. Tang, A novel hybrid process of reverse electrodialysis and reverse osmosis for low energy seawater desalination and brine management, Appl. Energy. 104 (2013) 592–602. doi:10.1016/j.apenergy.2012.11.064.

[7] M. Elimelech, W.A. Phillip, The future of seawater desalination: energy, technology, and the environment., Science. 333 (2011) 712–717. doi:10.1126/science.1200488.

[8] L.F. Greenlee, D.F. Lawler, B.D. Freeman, B. Marrot, P. Moulin, Reverse osmosis desalination: Water sources, technology, and today's challenges, Water Res. 43 (2009) 2317–2348. doi:10.1016/j.watres.2009.03.010.

[9] L. Malaeb, G.M. Ayoub, Reverse osmosis technology for water treatment: State of the art review, Desalination. 267 (2011) 1–8. doi:10.1016/j.desal.2010.09.001.

[10] R. Semiat, Energy issues in desalination processes, Environ. Sci. Technol. 42 (2008) 8193–8201. doi:10.1021/es801330u.

[11] M. Vanoppen, G. Blandin, S. Derese, P. Le-Clech, J.W. Post, A.R.D. Verliefde, Salinity gradient power and desalination, in: Sustain. Energy from Salin. Gradients, 2016: pp. 281–313.

[12] G.Z. Ramon, B.J. Feinberg, E.M. V. Hoek, Membrane-based production of salinity-gradient power, Energy Environ. Sci. 4 (2011) 4423. doi:10.1039/c1ee01913a.

[13] D.A. Vermaas, D. Kunteng, M. Saakes, K. Nijmeijer, Fouling in reverse electrodialysis under natural conditions, Water Res. 47 (2013) 1289–1298. doi:10.1016/j.watres.2012.11.053.

[14] T. Rijnaarts, J. Moreno, M. Saakes, W.M. de Vos, K. Nijmeijer, Role of anion exchange membrane fouling in reverse electrodialysis using natural feed waters, Colloids Surfaces A Physicochem. Eng. Asp. 560 (2019) 198–204. doi:10.1016/j.colsurfa.2018.10.020.

[15] R.S. Kingsbury, F. Liu, S. Zhu, C. Boggs, M.D. Armstrong, D.F. Call, O. Coronell, Impact of natural organic matter and inorganic solutes on energy recovery from five real salinity gradients using reverse electrodialysis, J. Memb. Sci. 541 (2017) 621–632. doi:10.1016/j.memsci.2017.07.038.

[16] M. Vaselbehagh, H. Karkhanechi, R. Takagi, H. Matsuyama, Biofouling phenomena on anion exchange membranes under the reverse electrodialysis process, J. Memb. Sci. 530 (2017) 232–239. doi:10.1016/j.memsci.2017.02.036.

[17] E. Van Houtte, J. Verbauwhede, Operational experience with indirect potable reuse at the Flemish Coast, Desalination. 218 (2008) 198–207. doi:10.1016/j.desal.2006.08.028.

[18] Y. Choi, S. Vigneswaran, S. Lee, Evaluation of fouling potential and power density in pressure retarded osmosis (PRO) by fouling index, Desalination. 389 (2016) 215–223. doi:10.1016/j.desal.2016.01.011.

[19] J. Luque Di Salvo, A. Cosenza, A. Tamburini, G. Micale, A. Cipollina, Long-run operation of a reverse electrodialysis system fed with wastewaters, J. Environ. Manage. 217 (2018) 871–887. doi:10.1016/j.jenvman.2018.03.110.

[20] D.A. Vermaas, D. Kunteng, J. Veerman, M. Saakes, K. Nijmeijer, Periodic feedwater reversal and air sparging as antifouling strategies in reverse electrodialysis, Environ. Sci. Technol. 48 (2014) 3065–3073.

[21] J. Moreno, N. de Hart, M. Saakes, K. Nijmeijer, CO2 saturated water as two-phase flow for fouling control in reverse electrodialysis, Water Res. 125 (2017) 23–31. doi:10.1016/j.watres.2017.08.015.

[22] P. Długołecki, J. Dabrowska, K. Nijmeijer, M. Wessling, Ion conductive spacers for increased power generation in reverse electrodialysis, J. Memb. Sci. 347 (2010) 101–107. doi:10.1016/j.memsci.2009.10.011.

[23] J. Moreno, E. Slouwerhof, D.A. Vermaas, M. Saakes, K. Nijmeijer, The Breathing Cell: Cyclic Intermembrane Distance Variation in Reverse Electrodialysis, Environ. Sci. Technol. 50 (2016) 11386–11393. doi:10.1021/acs.est.6b02668.

[24] J. Liu, G.M. Geise, X. Luo, H. Hou, F. Zhang, Y. Feng, M.A. Hickner, B.E. Logan, Patterned ion exchange membranes for improved power production in microbial reverse-electrodialysis cells, J. Power Sources. 271 (2014) 437–443.

[25] D.A. Vermaas, M. Saakes, K. Nijmeijer, Power generation using profiled membranes in reverse electrodialysis, J. Memb. Sci. 385–386 (2011) 234–242. doi:10.1016/j.memsci.2011.09.043.

[26] E. Güler, W. van Baak, M. Saakes, K. Nijmeijer, Monovalent-ion-selective membranes for reverse electrodialysis, J. Memb. Sci. 455 (2014) 254–270. doi:10.1016/j.memsci.2013.12.054.

[27] E. Bar-Zeev, N. Belkin, B. Liberman, T. Berman, I. Berman-Frank, Rapid sand filtration

pretreatment for SWRO: Microbial maturation dynamics and filtration efficiency of organic matter, Desalination. 286 (2012) 120–130. doi:10.1016/j.desal.2011.11.010.

[28] J.S. Vrouwenvelder, S.A. Manolarakis, J.P. van der Hoek, J.A.M. van Paassen, W.G.J. van der Meer, J.M.C. van Agtmaal, H.D.M. Prummel, J.C. Kruithof, M.C.M. van Loosdrecht, Quantitative biofouling diagnosis in full scale nanofiltration and reverse osmosis installations, Water Res. 42 (2008) 4856–4868. doi:10.1016/j.watres.2008.09.002.

[29] emis VITO, Sand filtration, (2010). https://emis.vito.be/en/techniekfiche/sand-filtration (accessed November 22, 2018).

[30] emis VITO, Microfiltration, (2010). https://emis.vito.be/en/techniekfiche/microfiltration (accessed December 10, 2018).

[31] C. Hoppe-Jones, E.R.V. Dickenson, J.E. Drewes, The role of microbial adaptation and biodegradable dissolved organic carbon on the attenuation of trace organic chemicals during groundwater recharge, Sci. Total Environ. 437 (2012) 137–144. doi:10.1016/j.scitotenv.2012.08.009.

[32] J.P. Van Der Hoek, C. Bertelkamp, A.R.D. Verliefde Bertelkamp, N. Singhal, Drinking water treatment technologies in Europe: State of the art - Challenges - Research needs, J. Water Supply Res. Technol. - AQUA. 63 (2014) 124–130. doi:10.2166/aqua.2013.007.

[33] M. Dubois, K.A. Gilles, J.K. Hamilton, P.A. Rebers, F. Smith, Colorimetric method for determination of sugars and related substances, Anal. Chem. 28 (1956) 350–356.

[34] J. Philips, K. Rabaey, D.R. Lovley, M. Vargas, Biofilm formation by clostridium ljungdahlii is induced by sodium chloride stress: Experimental evaluation and transcriptome analysis, PLoS One. 12 (2017) 1–25. doi:10.1371/journal.pone.0170406.

[35] X. Zhang, J. Philips, H. Roume, K. Guo, K. Rabaey, A. Prévoteau, Rapid and Quantitative Assessment of Redox Conduction Across Electroactive Biofilms by using Double Potential Step Chronoamperometry, ChemElectroChem. 4 (2017) 1026–1036. doi:10.1002/celc.201600853.

[36] J.B.A. Arends, E. Blondeel, S.R. Tennison, N. Boon, W. Verstraete, Suitability of granular carbon as an anode material for sediment microbial fuel cells, J. Soils Sediments. 12 (2012) 1197–1206. doi:10.1007/s11368-012-0537-6.

[37] L. Gutierrez, A. Keucken, C. Aubry, N. Zaouri, B. Teychene, J.P. Croue, Impact of operation conditions, foulant adsorption, and chemical cleaning on the nanomechanical properties of ultrafiltration hollow fiber membranes, Colloids Surfaces A Physicochem. Eng. Asp. 549 (2018) 34–42. doi:10.1016/j.colsurfa.2018.04.003.

[38] H.J. Butt, B. Cappella, M. Kappl, Force measurements with the atomic force microscope: Technique, interpretation and applications, Surf. Sci. Rep. 59 (2005) 1–152. doi:10.1016/j.surfrep.2005.08.003.

[39] L. Gutierrez, C. Aubry, L. Dramas, P. Aimar, J.P. Croue, Characterization of Skeletonema costatum intracellular organic matter and study of nanomechanical properties under different solution conditions, Colloids Surfaces A Physicochem. Eng. Asp. 506 (2016) 154–161. doi:10.1016/j.colsurfa.2016.06.025.

[40] N. Zaouri, L. Gutierrez, L. Dramas, D. Garces, J.P. Croue, Interfacial interactions between

Skeletonema costatum extracellular organic matter and metal oxides: Implications for ceramic membrane filtration, Water Res. 116 (2017) 194–202. doi:10.1016/j.watres.2017.03.034.

[41] B.V. Derjaguin, V.M. Muller, Y.V. Toporov, Effect of contact deformations on the adhesion of particles, J. Colloid Interface Sci. 53 (1975). doi:10.1016/0079-6816(94)90044-2.

[42] L. Gutierrez, A. Keucken, C. Aubry, T. Vera, S. Martin, Nanomechanical characterization of recalcitrant foulants and hollow fiber membranes in ultrafiltration systems, Desalin. Water Treat. 23257 (2018) 1–16. doi:10.5004/dwt.2018.23257.

[43] K.H. Mistry, H.A. Hunter, J.H. Lienhard V, Effect of composition and nonideal solution behavior on desalination calculations for mixed electrolyte solutions with comparison to seawater, Desalination. 318 (2013) 34–47. doi:10.1016/j.desal.2013.03.015.

[44] S. Pawlowski, T. Rijnaarts, M. Saakes, K. Nijmeijer, J.G. Crespo, S. Velizarov, Improved fluid mixing and power density in reverse electrodialysis stacks with chevron-profiled membranes, J. Memb. Sci. 531 (2017) 111–121. doi:10.1016/j.memsci.2017.03.003.

[45] D.A. Vermaas, M. Saakes, K. Nijmeijer, Doubled power density from salinity gradients at reduced intermembrane distance, Environ. Sci. Technol. 45 (2011) 7089–7095. doi:10.1021/es2012758.

[46] J.W. Post, C.H. Goeting, J. Valk, S. Goinga, J. Veerman, H.V.M. Hamelers, Towards implementation of reverse electrodialysis for power generation from salinity gradients, Desalin. Water Treat. 16 (2010) 182–193.

[47] P. Dlugolecki, K. Nymeijer, S. Metz, M. Wessling, Current status of ion exchange membranes for power generation from salinity gradients, J. Memb. Sci. 319 (2008) 214–222.

[48] H. Yamamura, K. Kimura, T. Okajima, H. Tokumoto, Y. Watanabe, Affinity of functional groups for membrane surfaces: Implications for physically irreversible fouling, Environ. Sci. Technol. 42 (2008) 5310–5315. doi:10.1021/es800406j.

[49] T. Merle, L. Dramas, L. Gutierrez, V. Garcia-Molina, J.P. Croué, Investigation of severe UF membrane fouling induced by three marine algal species, Water Res. 93 (2016) 10–19. doi:10.1016/j.watres.2016.02.001.

[50] L.C. Powell, N. Hilal, C.J. Wright, Atomic force microscopy study of the biofouling and mechanical properties of virgin and industrially fouled reverse osmosis membranes, Desalination. 404 (2017) 313–321. doi:10.1016/j.desal.2016.11.010.

[51] L. Gutierrez, C. Aubry, R. Valladares Linares, J.P. Croue, Natural organic matter interactions with polyamide and polysulfone membranes: Formation of conditioning film, Colloids Surfaces A Physicochem. Eng. Asp. 477 (2015) 1–8. doi:10.1016/j.colsurfa.2015.03.031.

[52] C. Bertelkamp, J.P. van der Hoek, K. Schoutteten, L. Hulpiau, L. Vanhaecke, J. Vanden Bussche, A.J. Cabo, C. Callewaert, N. Boon, J. Löwenberg, N. Singhal, A.R.D. Verliefde, The effect of feed water dissolved organic carbon concentration and composition on organic micropollutant removal and microbial diversity in soil columns simulating river bank filtration, Chemosphere. 144 (2016) 932–939. doi:10.1016/j.chemosphere.2015.09.017.

[53] C. Bertelkamp, A.R.D. Verliefde, K. Schoutteten, L. Vanhaecke, J. Vanden Bussche, N. Singhal, J.P. van der Hoek, The effect of redox conditions and adaptation time on organic micropollutant removal during river bank filtration: A laboratory-scale column study, Sci. Total Environ. 544

(2016) 309–318. doi:10.1016/j.scitotenv.2015.11.035.

[54] D. Li, M. Alidina, M. Ouf, J.O. Sharp, P. Saikaly, J.E. Drewes, Microbial community evolution during simulated managed aquifer recharge in response to different biodegradable dissolved organic carbon (BDOC) concentrations, Water Res. 47 (2013) 2421–2430. doi:10.1016/j.watres.2013.02.012.